Gamma rays from dark matter minispikes in the Andromeda Galaxy M31

Mattia Fornasa, Marco Taoso, Gianfranco Bertone

Gamma rays from dark matter minispikes in the Andromeda Galaxy M31

Mattia Fornasa,[1,*] Marco Taoso,[1,†] and Gianfranco Bertone[1,2,‡]

[1]*INFN, Sezione di Padova, via Marzolo 8, Padova, 35131, Italy*

[2]*Institut d Astrophysique de Paris, UMR 7095-CNRS, Université Pierre et Marie Curie, 98bis boulevard Arago, 75014 Paris, France*

(Received 5 April 2007; published 22 August 2007)

The existence of a population of wandering intermediate mass black holes (IMBHs) is a generic prediction of scenarios that seek to explain the formation of supermassive black holes in terms of growth from massive seeds. The growth of IMBHs may lead to the formation of DM overdensities called ''mini-spikes,'' recently proposed as ideal targets for indirect DM searches. Current ground-based gamma-ray experiments, however, cannot search for these objects due to their limited field of view, and it might be challenging to discriminate mini-spikes in the Milky Way from the many astrophysical sources that GLAST is expected to observe. We show here that gamma-ray experiments can effectively search for IMBHs in the nearby Andromeda Galaxy (also known as M31), where mini-spikes would appear as a distribution of point-sources, isotropically distributed in a $\approx 3^\circ$ circle around the galactic center. For a neutralinolike DM candidate with a mass $m_\chi = 150$ GeV, up to 20 sources would be detected with GLAST (at 5σ, in 2 months). With air Cherenkov telescopes such as MAGIC and VERITAS, up to 10 sources might be detected, provided that the mass of neutralino is in the TeV range or above.

DOI: 10.1103/PhysRevD.76.043517 PACS numbers: 95.35.+d, 97.60.Lf, 98.56.Ne, 98.70.Rz

I. INTRODUCTION

The nature of dark matter (DM) is, more than 70 years after its discovery, still an open problem. It is commonly assumed that DM is made of weakly interacting massive particles (WIMPs), arising in theories beyond the standard model (see Refs. [1,2] for recent reviews), the most widely discussed DM candidates being the supersymmetric neutralino and the lightest Kaluza-Klein particle (LKP) in theories with unified extra-dimensions [3–5]. These particles will be actively searched for in upcoming high energy physics experiments such as the Large Hadron Collider (LHC, see e.g. Refs. [5–8] for recent discussions in the context of DM searches), while hints on the nature of DM may already come from direct detection experiments aiming at detecting the nuclear recoils due to DM scattering off nuclei in large detectors (see e.g. Ref. [9] for a recent update on the status of direct searches). Alternatively, one could search for DM *indirectly*, i.e. through the detection of its annihilation products such as photons, neutrinos, positrons, and antiprotons. The annihilation rate being proportional to the square of the DM density, ideal targets of indirect searches include all those regions where the DM density is strongly enhanced, due to gravitational clustering, as in the case of the Galactic center [10–16] and halo substructures [17–25], or because of energy losses capture in large celestial bodies, as in the case of the Sun and the Earth (see Ref. [2], and references therein).

Large DM overdensities can also form as a consequence of astrophysical processes, such as the adiabatic growth of supermassive [26–28] or intermediate mass black holes [29,30]. In fact, DM halos inevitably react to the growth of black holes, leading, in the case of adiabatic growth, to the formation of large DM overdensities called *spikes* [26]. A DM cusp with a power-law density profile $\rho \propto r^{-\gamma}$, gets redistributed after the BH growth into a steeper profile $\rho_{sp} \propto r^{-\gamma_{sp}}$, with $\gamma_{sp} = (9 - 2\gamma)/(4 - \gamma)$, within the radius of gravitational influence of the black hole (BH) (see below for further details). BHs can thus be thought as *annihilation boosters*, because the annihilation rate after their growth is boosted by several orders of magnitude, making these objects ideal targets for indirect DM searches. Even in absence of mergers [31], and ignoring a possible off-center formation [32], a spike around the Supermassive BH at the Galactic center would inevitably be destroyed by the combined effect of gravitational scattering off the *observed* stellar cusp at the GC, and DM annihilations [14]. The very same gravitational processes can still lead to the formation of moderate enhancements called collisionally regenerated structures (CRESTS), but these structures do not lead to significant enhancements of the annihilation signal [33]. *Mini-spikes* around intermediate mass black holes (IMBHs) are more promising targets of indirect detection, since they would not be affected by these dynamical processes, and they should appear as bright pointlike sources, which could be easily detected by large field of view gamma-ray experiments as GLAST [34] and further studied with ground-based air Cherenkov telescopes (ACTs) [30] such as CANGAROO [35], HESS [36], MAGIC [37], and VERITAS [38]. Here, we further explore the mini-spikes scenario, and focus on the population of IMBHs in the Andromeda Galaxy (also known as M31), a spiral galaxy very similar to the Milky Way (MW), whose center is located 784 kpc away from us. We compute gamma-ray fluxes from DM annihilations around IMBHs in M31, and show that the prospects for detection

*nmfornasa@pd.infn.it
†taoso@pd.infn.it
‡gianfranco.bertone@pd.infn.it

with GLAST are very promising: in an optimistic case (a neutralino with a mass $m_\chi = 150$ GeV and annihilation cross section $\sigma v = 3 \times 10^{-26}$ cm^3 s^{-1}), GLAST may detect up to 20 pointlike sources (at 5σ and with a 2 months exposure), within 3° from the center of Andromeda. The proposed observational strategy appears particularly suited for ACTs like MAGIC and VERITAS, (M31 is in a region of the sky not accessible to HESS), since the main difficulty in the search for Galactic mini-spikes is that they cannot perform *deep* full-sky searches, due to their limited field of view. In the case of mini-spikes in M31, ACTs can search for them by scanning a small region of $\approx 3°$ around the center of M31, and an effective exposure of ≈ 100 hours in this region would be sufficient to probe the proposed scenario, at least for DM mass in the TeV range. The next-generation Cherenkov telescopes array (CTA)[39], is expected to significantly improve the sensitivity, increase the field of view and decrease the energy threshold with respect to existing ACTs, thus representing an ideal experiment for the proposed scenario.

The paper is organized as follows: next section (Sec. II) is devoted to describe the formation scenario of IMBHs. We then (Sec. III) present the IMBHs catalogue and how it is adapted to the Andromeda Galaxy. We compute the gamma-ray flux emitted by each pointlike spike around an IMBH, considering a particular energy annihilation spectrum for a DM particle. In Sec. IV A we estimate the prospects for detection for a generic ACT. Then in Sec. IV B we turn to GLAST. Finally our results are discussed in Sec. V.

II. INTERMEDIATE MASS BLACK HOLES

A. IMBHs formation scenario

IMBHs are compact objects with mass larger than $\approx 20M_\odot$, the heaviest remnant of a stellar collapse [40], and smaller than $\approx 10^6 M_\odot$, the lower end of the mass range of supermassive black holes (SMBH) [41]. The theoretical and observational motivations for IMBHs were recently reviewed in Ref. [42]. For instance, ultraluminous x-ray point sources (ULXs) could be interpreted as accreting IMBHs, since alternative explanations in terms of AGNs, neutron stars or SMBHs appear to be problematic or even ruled out [42,43].

From a theoretical point of view, a population of massive seed black holes could help to explain the origin of SMBHs. In fact, observations of quasars at redshift $z \approx 6$ in the Sloan digital survey [44–46] suggest that SMBHs were already in place when the Universe was only $\sim$1 Gyr old, a circumstance that can be understood in terms of rapid growth starting from massive seeds (see e.g. Ref. [47]).

In fact, a generic prediction of scenarios that seek to explain the properties of the observed supermassive black hole population, is that a large number of ''wandering'' IMBHs should exist in DM halos [48–50]. Despite their theoretical interest, it is difficult to obtain conclusive evidence for the existence of IMBHs. A viable detection strategy could be the search for gravitational waves produced in the mergers of the IMBH population [51–56], with space-based interferometers such as LISA [57].

In Ref. [30], two scenarios for IMBHs formation have been considered. The first posits IMBHs as remnants of the collapse of Population III stars. These are stars with very low metallicity, that do not experience any metal line cooling, leading to a higher mass scale with respect to more recent stars. Moreover, they do not have significant winds, and have weak pulsations, so that they lose comparatively little of their mass during the evolution. Stars heavier than $250M_\odot$ collapse directly to a BH without any mass loss [42], and under some simplifying assumptions, a population of roughly 1000 IMBHs with mass of 10^2–$10^3 M_\odot$ is predicted to wander in the MW DM halo [30].

Here, we will focus only on the second scenario, based on Ref. [49], where IMBHs form at high redshift from gas collapsing in mini-halos. If the latter are massive enough, protogalactic disks form at the center of each halo, composed by baryons lying in the low values tail of the angular momentum distribution. Gravitational instabilities introduce an effective viscosity that causes an inward mass and an outward angular momentum flow. The process goes on until it is interrupted by feedback from star formation (1–10 Myrs) that heats the disk. Then the so-formed object undergoes gravitational collapse into a black hole. A characteristic mass scale of $10^7 M_\odot$ is imprinted to the mini-halo by the requirements that it is heavy enough to form a gravitational unstable disc and that the black hole formation timescale is shorter than the typical major mergers one. The resulting black holes have a mass log-normally scattered, with a $\sigma_\bullet = 0.9$, around the mean value of Ref. [49]:

$$M_\bullet = 3.8 \times 10^4 M_\odot \left(\frac{\kappa}{0.5}\right)\left(\frac{f}{0.03}\right)^{3/2}\left(\frac{M_{\rm vir}}{10^7 M_\odot}\right) \times \left(\frac{1+z}{18}\right)^{3/2}\left(\frac{t}{10\ {\rm Myr}}\right), \quad (1)$$

where κ is that fraction of the baryonic mass which loses its angular moment that remains in the remnant black hole. f is the fraction of the total baryonic mass in the halo that has fallen into the disc, $M_{\rm vir}$ is the halo virial mass, z is the redshift of formation and t the timescale for the evolution of the first generation of stars.

Although our analysis is performed in the context of this specific scenario, it is by no means assured that this is the actual mechanism for IMBHs formation. The recipe for halo population and spike formation can nevertheless be generalized to any IMBHs formation scenario.

In Ref. [30] Bertone *et al.* have studied the population of IMBHs in the MW, following the evolution of mini-halos hosting IMBHs at high redshift (populated with the prescriptions of Ref. [49]), down to redshift $z = 0$ (see

Ref. [30] for further details). As a result, they obtained 200 realizations of the IMBHs population in the Galaxy, that were used to produce 200 mock catalogs of DM minispikes, and to study the prospects for detection of these objects in the Galaxy. The average number of unmerged IMBHs was found to be $\overline{N} = 101 \pm 22$, and each of these objects is characterized by its mass, distance from the center of the galaxy, and surrounding DM distribution.

B. DM distribution around IMBHs

Following earlier work on the dynamics of stars and DM around compact objects (see Ref. [58] and references therein), Gondolo and Silk have shown that the adiabatic growth of a massive black hole in the center of a dark halo modifies the distribution of the surrounding DM, inducing an enhancement of the density called "spike" [26]. They focused their attention on the SMBH at the center of our Galaxy, but the same formalism can be applied also to IMBHs. The initial DM distribution in all mini-halos can be adequately parametrized with a Navarro, Frenk, and White (NFW) profile [59]:

$$\rho(r) = \rho_0 \left(\frac{r_s}{r}\right)\left(1 + \frac{r}{r_s}\right)^{-2}, \tag{2}$$

where r_s, called the scale radius, sets the radius at which the profile slope changes. The new profile after the adiabatic growth, will be [26]:

$$\rho_{\rm sp}(r) = \rho(r_{\rm sp})\left(\frac{r}{r_{\rm sp}}\right)^{-7/3}, \tag{3}$$

where ρ is the density function of the initial NFW profile. r_{sp} gives the upper limit inside which Eq. (3) is considered valid and is related to the radius of gravitational influence of the black hole r_h: $r_{\rm sp} \approx 0.2 r_h$ [60], where r_h is implicitly defined as

$$M(r < r_h) \equiv \int_0^{r_h} \rho(r) r^2 dr = 2M_\bullet$$

with $M_\bullet$ is the mass of the black hole.

The spike profile diverges at low radii but annihilations set an upper limit to the physical density. Solving the evolution of the DM particles number density, one finds that the upper limit depends on the microphysical properties of the DM particles (mass and annihilation cross section) and on the evolution timescale of the black hole. We denote the distance where the density equals this upper limit $r_{\rm lim}$, and following Ref. [30] we define a cut-radius for our density profiles:

$$r_{\rm cut} = {\rm Max}[4R_{\rm Schw}, r_{\rm lim}], \tag{4}$$

where $R_{\rm Schw} = 2.95\ {\rm km}\, M/M_\odot$ is the BH Schwarzschild radius. The density between $R_{\rm Schw}$ and $r_{\rm cut}$ is assumed to be constant to $\rho_{\rm sp}(r_{\rm cut})$.

Although we perform our calculations in the context of NFW profiles, we note that spike slope $\gamma_{\rm sp}$ depends weakly on the initial slope γ:

$$\gamma_{\rm sp} = \frac{9 - 2\gamma}{4 - \gamma}. \tag{5}$$

Varying γ between 0 to 1.5, $\gamma_{\rm sp}$ thus ranges between 2.25 to 2.4. Furthermore, although the spike depends quite strongly on the density normalization at $r_{\rm sp}$, most alternative profiles deviate from NFW on scales smaller than $r_{\rm sp}$. We have for instance checked the case of the Navarro *et al.* profile proposed in Ref. [61] and found that the corresponding annihilation flux from each spike gets rescaled only by a factor 1.6, which is well within the other uncertainties in our calculations.

III. GAMMA-RAYS FROM IMBHS IN M31

A. IMBHs in M31

Although similar, the Milky Way and Andromeda do not have exactly the same properties. The mock catalogs of IMBHs built for our Galaxy, thus have to be modified to account for the different average number and different spatial distribution in the host halo. A comparison between the properties of Andromeda and of the Galaxy is shown in Table I.

We start from the mock catalogs obtained in Ref. [30] and we rescale the total number of objects by the ratio between the host halo masses, since the number of unmerged IMBHs scales linearly with the host halo mass, and the galactocentric distance by the ratio of virial radii. We obtain for M31 an average number of IMBHs per realization $N_{M31} = 65.2 \pm 14.5$. The mass spectrum remains unchanged, with an average mass around $10^5 M_\odot$, while the average distance from the center of the galaxy is 32.31 kpc. We have verified that our rescaling procedure reproduces in a satisfactory way the properties of the IMBHs population in Andromeda, by comparing our results with a limited number of mock catalogs obtained as an exploratory study in Ref. [30].

TABLE I. Distance from the Sun (in kpc), virial radius (defined as the radius within which the density reaches 200 times the critical density, in kpc), virial mass (in solar masses) and the two NFW density profile parameters (in kpc and $M_\odot\,{\rm kpc}^{-3}$ respectively), both for the MW and the Andromeda Galaxy [62,63].

	Milky Way	Andromeda
Distance to the center [kpc]	8.5	784.0
Virial Radius [kpc]	205	180
Virial Mass [$M_\odot$]	1.0×10^{12}	6.8×10^{11}
r_s [kpc]	21.75	8.18
ρ_0 [$\frac{M_\odot}{\rm kpc^3}$]	5.376×10^6	3.780×10^7

B. Gamma-rays flux from IMBHs in M31

Once the mock catalogs of IMBHs in M31 have been obtained, it is possible to calculate the gamma-ray flux from each IMBH in every realization. The calculation follows Eq. (14) in Ref. [30]:

$$\Phi(E) = \frac{\sigma v}{2m_\chi^2}\frac{1}{d^2}\frac{dN_\gamma(E)}{dE}\int_{r_{\rm cut}}^{r_{\rm sp}}\rho^2(r)r^2dr$$
$$= \Phi_0\frac{dN_\gamma(E)}{dE}\left(\frac{\sigma v}{10^{-26}\ {\rm cm}^3/{\rm s}}\right)\left(\frac{m_\chi}{1\ {\rm TeV}}\right)^{-2}$$
$$\times\left(\frac{d}{780\ {\rm kpc}}\right)^{-2}\left(\frac{\rho(r_{\rm sp})}{100\ {\rm GeV/cm}^3}\right)^2$$
$$\times\left(\frac{r_{\rm sp}}{5\ {\rm pc}}\right)^{14/3}\left(\frac{r_{\rm cut}}{10^{-3}\ {\rm pc}}\right)^{-5/3}, \quad (6)$$

where $\Phi_0 = 2.7\times10^{-14}\ {\rm cm}^{-2}\,{\rm s}^{-1}$, d is the IMBH distance to the observer, σv is the DM annihilation cross section times relative velocity and m_χ is the DM particle mass (the letter χ, usually adopted for neutralino, is used here to denote a generic WIMP candidate). $r_{\rm cut}$ and $r_{\rm sp}$, represent the inner and outer size of the spike, as discussed in the previous section.

$dN_\gamma(E)/dE$ is the differential photon yield per annihilation, that can be expressed as:

$$\frac{dN_\gamma(E)}{dE} = \sum_a B^a\frac{dN_\gamma^a(E)}{dE}. \quad (7)$$

Common DM candidates can annihilate into a pair of SM particles $a\bar{a}$ where a stands for a fermion or a gauge or Higgs boson. The ratio of the annihilation rate into a particular channel $a\bar{a}$ over the total annihilation rate is called Branching ratio B^a. dN_γ^a/dE is the secondary photon spectrum due to the annihilation channel $a\bar{a}$. The latter term is thus a purely standard model calculation, while branching ratios have to be derived in the framework of new theories beyond the Standard Model, such as SUSY or UED.

We review here different parametrizations of the photon yield that have been recently proposed in literature. The first parametrization we focus on, has been obtained in Ref. [62], and it is relative to annihilations into $b\bar{b}$. The authors have parametrized the results obtained with the event generator PYTHIA [64] as follows:

$$\frac{dN_\gamma^b(x)}{dx} = x^a e^{b+cx+dx^2+ex^3}, \quad (8)$$

where the parameters depend on the neutralino mass, and for the specific case $m_\chi = 1$ TeV, $(a, b, c, d, e) = (-1.5, 0.37, -16.05, 18.01, -19.50)$. While for annihilation to τs

$$\frac{dN_\gamma^\tau(x)}{dx} = x^a(bx + cx^2 + dx^3)e^{ex}, \quad (9)$$

and for $m_\chi = 1$ TeV, $(a, b, c, d, e) = (-1.31, 6.94, -4.93, -0.51, -4.53)$.

Alternatively, one can start from the most recent Fragmentations Functions (FFs) (e.g. Ref. [65]), describing the hadronization of partons into the particles of interest. The FF of b quarks hadronizing in neutral pions has been fitted with a simple analytic form that captures in a satisfactory way the behavior of the FF at large x finding the following analytic fit

$$f(x) = \frac{7.53}{x^{0.87}e^{14.62x}}. \quad (10)$$

Convolving the spectrum pions with their decay spectrum into photons one finally obtains the differential photon yield

$$\frac{dN_\gamma(x)}{dx} = \int_x^1 f(x')\frac{2}{x'}dx'. \quad (11)$$

We have also considered an example inspired from theories with unified extra dimensions, where the role of DM is usually played by the first excitation of the hypercharge gauge boson, and referred to as $B^{(1)}$. Since the $B^{(1)}$ annihilation into fermions does not suffer from chirality suppression, as in MSSM, we also include the contribution from annihilation to $l\bar{l}\gamma$, as calculated in Ref. [66], as well as the contribution from τ fragmentation, and usual from annihilations to $b\bar{b}$, with the appropriate branching ratio. The final state radiation arising from annihilation to charged leptons has a characteristic, very hard, spectral

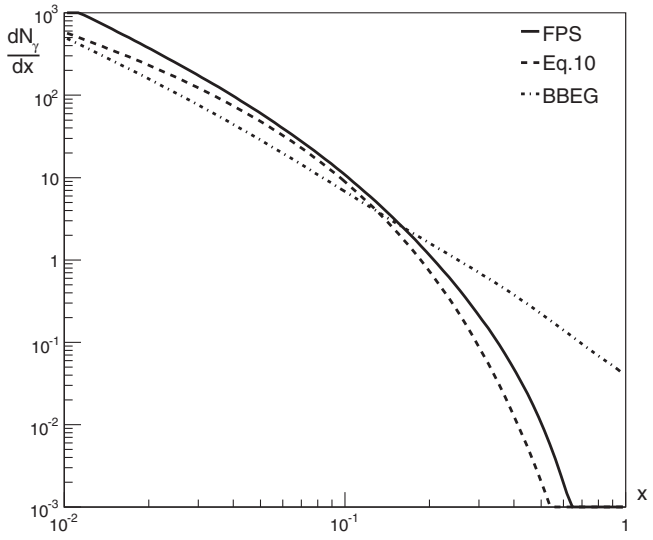

FIG. 1. Differential photon spectrum per annihilation. Different parametrizations and annihilation channels are shown. Solid line (FPS) is an analytic fit relative to the $b\bar{b}$ channel, as obtained in Eq. (8). Dashed line [Eq. (11)] is relative to the same annihilation channel $b\bar{b}$, but with a different parametrization of the FFs [see Eqs. (10) and (11)]. Dotted line (BBEG) is relative to B^1 annihilations and includes final state radiation from annihilation to charged leptons [66] (see text for more details).

TABLE II. Gamma-ray flux over 100 GeV from Andromeda (in $cm^{-2}\,s^{-1}$) for a smooth NFW, and for the different parametrizations discussed in the text. Differences among the predicted fluxes are within a factor of 2.

	M31 flux [$cm^{-2}\,s^{-1}$]
FPS [62]	1.33×10^{-14}
Equation (11)	9.79×10^{-15}
BBEG [66]	1.60×10^{-14}

shape [66,67]

$$\frac{dN_\gamma^l(x)}{dx} = \sum_{l=e,\mu} \frac{\alpha}{\pi} \frac{x^2 - 2x + 2}{x} \ln\left[\frac{m_{B^{(1)}}^2}{m_l^2}(1-x)\right]. \quad (12)$$

The three prescriptions for the annihilation spectrum are plotted in Fig. 1 (for $m_\chi = 1$ TeV). As expected, all spectra are very similar up to $x \equiv E/m_\chi \sim 0.1$, but the spectrum relative to $B^{(1)}$ annihilations is harder at large x, and exhibits a distinctive sharp cutoff at $x = 1$.

To show the small effect that the adoption of different annihilation spectra has on the prospects for indirect detection, we have calculated the DM annihilation flux from the smooth component of the M31 halo, assuming a NFW profile with the parameters described in Table I above. The results are displayed in Table II, and as one can see, differences are within a factor of two. In the remain of this paper, we will thus work only with the first analytic fit, since the uncertainties associated with other astrophysical and particle physics parameters are significantly larger.

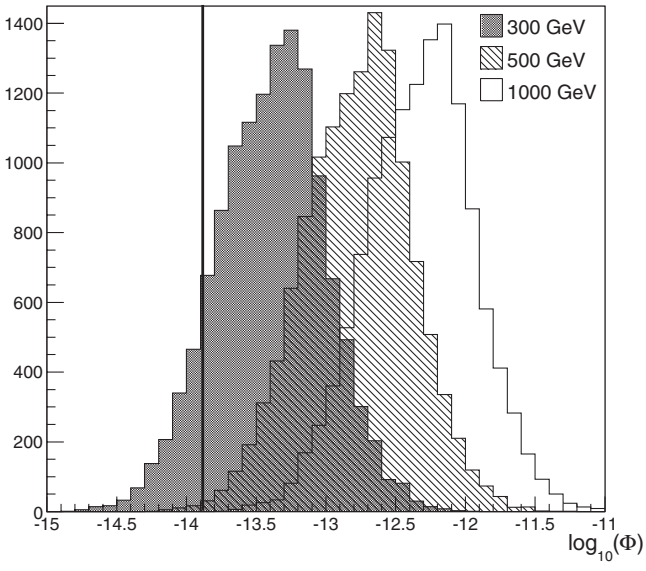

FIG. 2. Luminosity function of IMBHs (fluxes are in $cm^{-2}s^{-1}$), for $m_\chi = 0.3$, 0.5 and 1 TeV. Energy threshold is equal to 100 GeV and $\sigma v = 3 \times 10^{-26}\ cm^3\,s^{-1}$. The vertical line shows the contribution of the smooth component of the M31 halo, assuming a NFW profile and $m_\chi = 1$ TeV.

TABLE III. Average flux from IMBHs in all 200 realizations (in $cm^{-2}\,s^{-1}$), for different values of DM mass, $\sigma v = 3 \times 10^{-26}\ cm^3\,s^{-1}$ and $E_{thr} = 4$ GeV.

	Average flux [$cm^{-2}\,s^{-1}$]
$m_\chi = 50$ GeV	5.26×10^{-11}
$m_\chi = 150$ GeV	7.65×10^{-11}
$m_\chi = 300$ GeV	6.92×10^{-11}
$m_\chi = 500$ GeV	5.81×10^{-11}

By calculating the gamma-ray flux in Eq. (6) for IMBHs in all realizations, we obtain the luminosity function of IMBHs (sum of all realizations), for different values of the DM particle mass (see Fig. 2). The distribution is approximately gaussian, and the average flux of IMBHs is larger than emission due the smooth component. The dependence from the mass results in due to a balance between the $m_\chi^{-9/7}$ dependence in Eq. (6), and the m_χ dependence of the upper limit in the integral of the energy spectrum. Having set in the figure an energy threshold $E_{thr} = 100$ GeV, the luminosity flux towards higher fluxes when the mass increase. We will come back later to this threshold effect, that leads to higher fluxes for higher masses when $m_\chi \sim E_{thr}$ despite the explicit $m_\chi^{-9/7}$ dependence of the annihilation flux. Meanwhile we note that this effect disappears when $m_\chi \gg E_{thr}$, as can be seen from Table III.

IV. PROSPECTS FOR DETECTION

As we shall see the prospects for detection depend on the expected or measured experimental performances, but also on the atmospheric and astrophysical backgrounds. We perform separate analysis for air Cherenkov telescopes and the upcoming gamma-ray satellite GLAST.

A. Prospects for ACTs

The calculations in this section are performed for a generic ACT, but they are particularly relevant for two specific experiments: MAGIC and VERITAS. As for HESS, being located in Namibia, it cannot detect gamma rays from the direction of Andromeda.

To determine the significance of the signal from an individual mini-spike, as calculated in the previous section, we compare the number of signal photons, to the fluctuations of the background

$$n = \frac{n_\gamma}{\sqrt{n_{bk}}} = \sqrt{T \cdot \Delta\Omega}\, \frac{\int A_{eff}(E,\theta)\frac{d\Phi}{dE}\,dE d\theta}{\sqrt{\int A_{eff}(E,\theta)\frac{d\Phi_{bk}}{dE}\,dE d\theta}}, \quad (13)$$

where T is the exposure time, A_{eff} the effective area, $\Delta\Omega$ the solid angle, $d\Phi_{bk}/dE$ is the total background differential flux.

For air Cherenkov telescopes, the main background is due to hadrons interacting with the atmosphere and producing electromagnetic showers. Following Ref. [24,68],

we consider

$$\frac{d\Phi_h}{d\Omega dE} = 1.5 \times \left(\frac{E}{\mathrm{GeV}}\right)^{-2.74} \frac{\mathrm{p}}{\mathrm{cm}^2\,\mathrm{sGeVsr}}. \quad (14)$$

The ratio of the number of hadrons misinterpreted as gamma rays, over the total number of cosmic ray hadrons, ϵ_h, provides an estimate of the telescope potential to discriminate the gamma-ray signal from the hadronic background. We adopt a typical value $\epsilon_h = 10^{-2}$, following Refs. [24,69]. The electronic contribution to the background is [24]

$$\frac{d\Phi_e}{d\Omega dE} = 6.9 \times 10^{-2}\left(\frac{E}{\mathrm{GeV}}\right)^{-3.3} \frac{\mathrm{e}}{\mathrm{cm}^2\,\mathrm{sGeVsr}}, \quad (15)$$

and it is typically subdominant at the energies of interest.

In Fig. 3 we compare the DM annihilation signal with the different sources of background, as a function of the field of view. The minimum flux for a 5σ detection with an effective area of $A_{\mathrm{eff}} = 3 \times 10^4$ m^2 [37] and an exposure time of 100 hours, is $\phi_{\mathrm{min}} = 1.6 \times 10^{-12}$ cm^{-2} s^{-1}.

To produce this estimate we have considered values of effective area and angular resolution similar to MAGIC and the result is consistent with earlier estimates of the MAGIC sensitivity [2]. An actual estimate of the instrument performance suggests that the minimum flux can be up to an order of magnitude higher [70].

A sky-map for Andromeda (like in the left panel of Fig. 4) is obtained computing the fluxes from the minispikes in a random realization among the 200 of the mock catalogue. The pixel size matches the angular resolution of

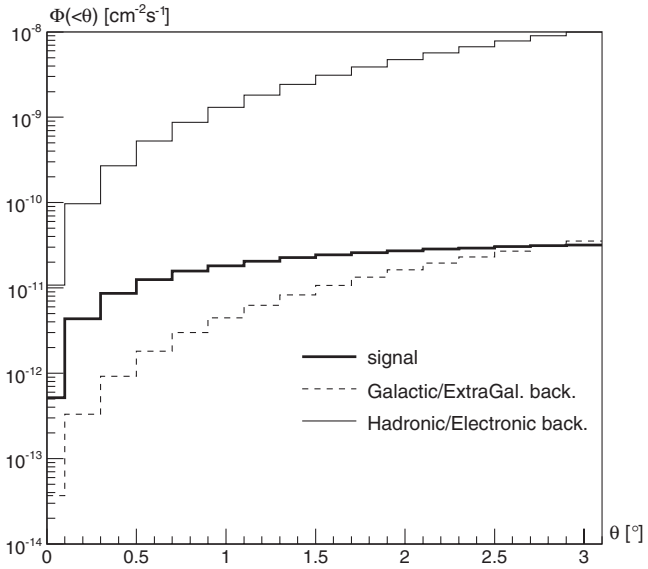

FIG. 3. Gamma-ray flux (in cm^{-2}s^{-1}) from DM annihilation around IMBHs (solid thick line), integrated over a cone of size θ towards the center of M31, as a function of θ. We show for comparison the hadronic/electron background, assuming $\epsilon_h = 10^{-2}$ (solid thinner line) and the diffuse extragalactic background (dashed line).

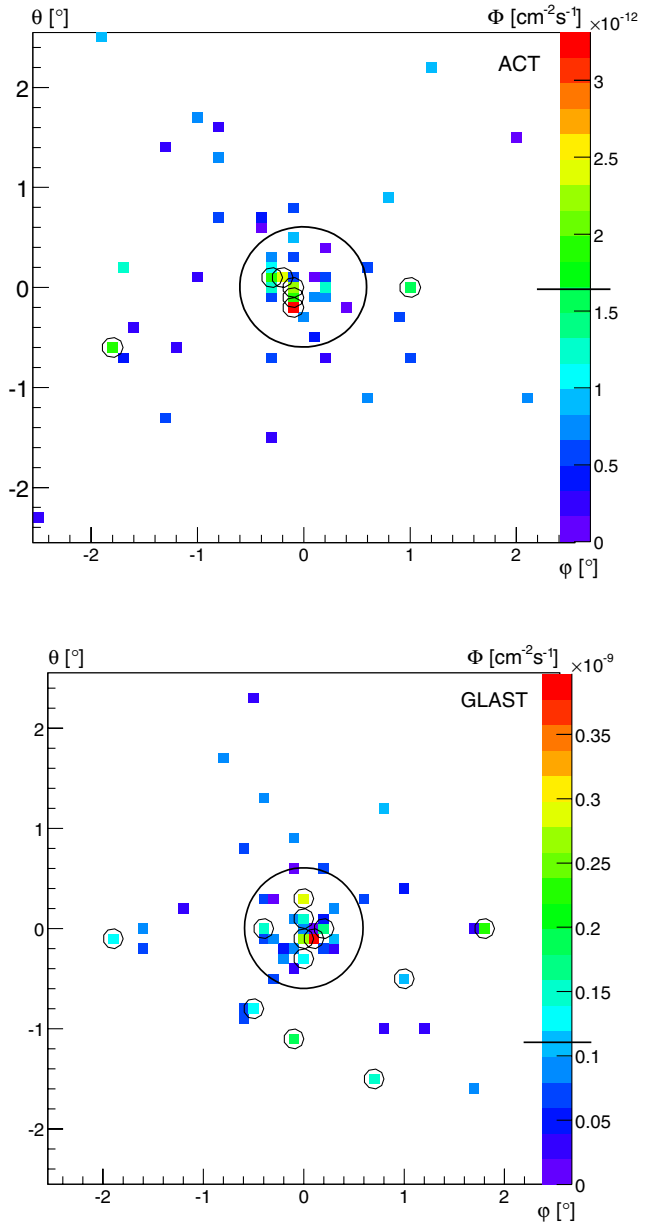

FIG. 4 (color online). Color online. Left (right) panel shows a map of the gamma-ray flux in units of photons cm^{-2} s^{-1}, from DM annihilations around IMBHs in M31, relative to one random realization of IMBHs in M31. The size of the bins is 0.1° and the threshold for the left (right) panel is 100 GeV (4 GeV) as appropriate for ACTs (GLAST). The circles highlight IMBHs within the reach of current ACTs for a 5σ detection in 100 hours (within the reach of GLAST for a 5σ detection in 2 months). The big circle shows for comparison the M31 scale radius r_s.

ground-based telescopes such as VERITAS and MAGIC, and of GLAST. For the map, a DM mass of 1 TeV and an annihilation cross section $\sigma v = 3 \times 10^{-26}$ cm^3 s^{-1} have been adopted. Black circles highlight the position of objects brighter than the experimental sensitivity (indicated in the color scale by the black line).

The number of detectable IMBHs (averaged above the 200 realizations) for $m_\chi = 1$ TeV is $N_{5\sigma} = 5.2 \pm 3.1$, where the error is relative to the 1-σ scatter in the computation of the average.

We note that current simulations indicate that the next-generation Cherenkov telescopes array (CTA) [39], may significantly improve the se nsitivity, down to $\phi_{\rm min} \approx 10^{-13}$ cm^{-2} s^{-1}, thus leading to a substantial improvement in the prospects for detection.

B. Prospects for GLAST

The space satellite GLAST is expected to play a crucial role in indirect DM searches, thanks both to its ability to perform observations at energy scales comparable to the mass of common DM candidates and to its potential of making deep full-sky maps in gamma rays, thanks to its large (~ 2.4 sr) field of view [34]. Despite the smaller effective area, it is not affected, being a satellite, by the atmospheric hadronic and electron background. Furthermore, its lower energy threshold (30 MeV) allows to probe lighter DM particles, typically leading to higher fluxes. The angular resolution of GLAST is $\approx 3°$ in the energy range 30 MeV–500 MeV, becomes 0.5 degrees from 500 MeV to 4 GeV, and reaches 0.15 degrees above 4 GeV [34].

As in the case of ACTs, we compare the expected fluxes with the photon background, which in this case, since GLAST will perform observations above the atmosphere, is mainly due to diffuse gamma-ray emission. The galactic and extragalactic background has been measured in Refs. [71,72] by EGRET in the energy range between 30 MeV and 10 GeV and we extrapolate it to higher energies by fitting with a power-law with spectral index of -2.1. The resulting formula is

$$\frac{d\Phi_{\rm extra/gal}}{d\Omega dE} = 2.3 \times 10^{-6} \left(\frac{E}{\rm GeV}\right)^{-2.1} \frac{\gamma}{\rm cm^2\, s\, GeV\, sr}. \quad (16)$$

We note here that a large fraction of the observed gamma-ray background might be actually due to DM annihilations [73–76], in particular, if astrophysical processes can boost the annihilation signal [77,78]. In this case, the smoking gun for this scenario would be the distinctive shape of the angular power-spectrum of the background, that may allow, already with GLAST, the discrimination against ordinary astrophysical sources [79].

The sensitivity above 30 MeV, i.e. the minimum detectable flux for a 5σ detection with an exposure of 2 months, is found to be $\phi_{\rm min} = 3.2 \times 10^{-8}$ cm^{-2} s^{-1}. This value is derived from Eq. (13), adopting values of the energy dependent effective area provided by Ref. [80], and is consistent with GLAST sensitivity maps obtained in Ref. [81]. The integral flux above threshold from IMBHs, averaged among realizations and integrated in a 3° cone towards M31, is $\phi_{30} = 1.3 \times 10^{-7}$ cm^{-2} s^{-1}.

In the right panel of Fig. 4, we show the results of our analysis relative to a random realization, and adopting $m_\chi = 150$ GeV, and $\sigma v = 3 \times 10^{-26}$ cm^3 s^{-1}. Mini-spikes appear as high emission peaks, and can be easily

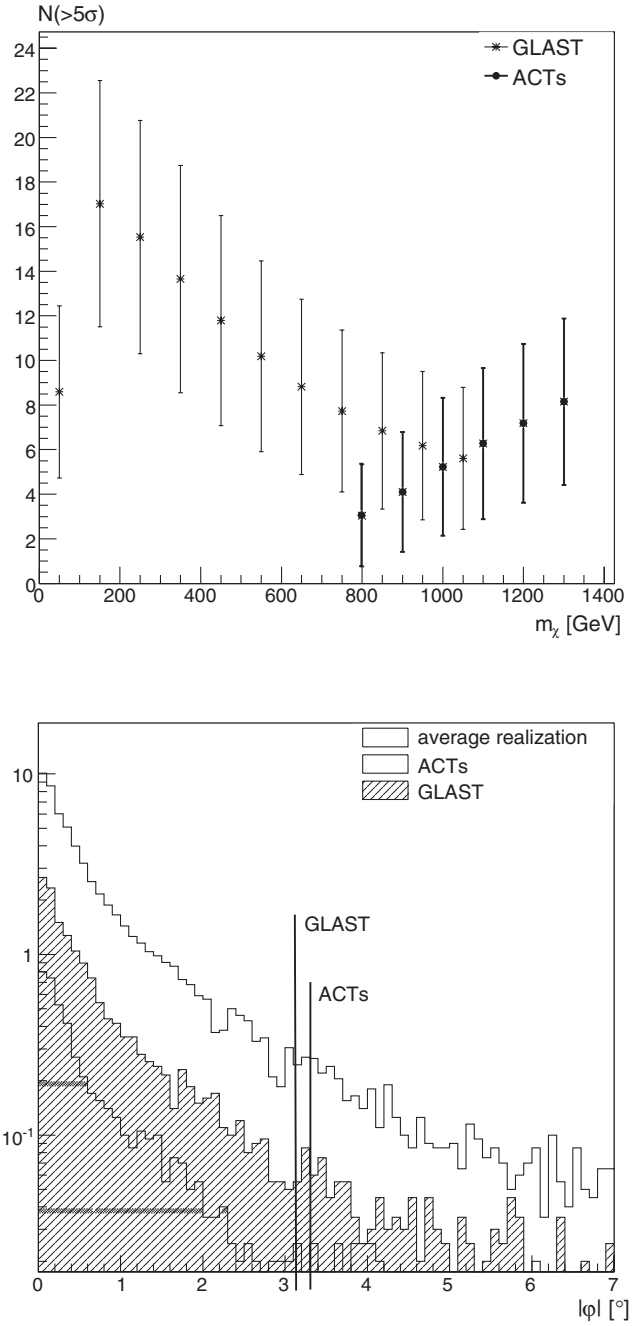

FIG. 5. Number of detectable mini-spikes in M31 with GLAST (2 months) and ACTs (100 hours) as a function of the DM particle mass (left) and as a function of the angular distance from the center of M31 (right). In the left panel, error bars denote the $1-\sigma$ scatter among different realizations. In the right panel, the total number of objects is shown as an empty histogram, while the vertical lines denote the size of the region that contains 90% of the detectable IMBHs.

resolved by selecting photons above 4 GeV, so that the angular resolution of GLAST approaches 0.1 degrees. Black circles highlight those objects that produce a flux detectable at 5σ with GLAST, with a 2 months exposure.

V. DISCUSSION AND CONCLUSIONS

Although we have performed the analysis of the prospects for detection with GLAST and ACTs for 2 different benchmark scenarios (essentially high DM particle mass for ACTs, low m_χ for GLAST), the analysis can be easily extended to any value of the particle physics parameters of the annihilating DM particle. To explore the dependence on m_χ, we show in the left panel of Fig. 5 the number of objects that can be detected with the aforementioned experiments, as a function of the DM particle mass. Near the experiment threshold, fluxes increase with mass. When $m_\chi \gg E_{\rm thr}$ this threshold effect disappears and one recovers the expected behavior (smaller fluxes for higher masses).

Similarly, one can plot the number of detectable objects as a function of the angular distance from the center of M31, to estimate the region where most mini-spikes can be found. This is shown in the right panel of Fig. 5 where the total number of objects is also shown for comparison. Vertical lines denote the angular size of the region that contains 90% of the detectable IMBHs for the various experiments, which has a characteristic size of $\theta = 3.3°$.

We stress that, while in the case of Galactic IMBHs the identification of mini-spikes will require a case-by-case analysis of their spectral properties, variability and multi-wavelength counterparts, as discussed in Ref. [25], for the IMBHs around Andromeda, the detection of a cluster of sources around the center of the galaxy would *per se* provide a hint on the nature of these sources, since other astrophysical sources, e.g. gamma-ray pulsars, will tend to lie in the disk and bulge of M31, while IMBHs would be isotropically distributed around its center, within a region of $\sim 3°$.

In conclusion, we have computed gamma-ray fluxes from DM annihilations in mini-spikes around IMBHs in the Andromeda Galaxy. We have studied the prospects for detection with air Cherenkov telescopes like MAGIC and VERITAS and with the GLAST satellite, and found that a handful of sources might be within the reach of current ACTs, while the prospects for the planned CTA are more encouraging. The obvious advantage of the proposed scenario with respect to mini-spikes in the MW, is that they are not randomly distributed over the sky, but they are contained, at 90%, within 3 degrees from the center of Andromeda, and can thus be searched for with ACTs by performing a deep scan of this small region.

The prospects for GLAST appear more promising, since an exposure time of 2 months allows the detection of up to of ≈ 20 mini-spikes, that would be resolved as a cluster of point-sources with identical spectra, within a $\sim 3°$ region around the center of Andromeda. Such a distinctive prediction cannot be mimicked by ordinary astrophysical sources. As in the case of IMBHs in the MW, null searches would place very strong constraints on the proposed scenario in a wide portion of the DM parameter space.

We thank Riccardo Rando, of the GLAST collaboration, as well as Mosè Mariotti and Michele Doro of the MAGIC Collaboration, for useful information and discussions on experimental strategies and sensitivities. We also thank Andrew Zentner for earlier collaboration and for providing the mock catalogs of IMBHs in the MW and Lidia Pieri for comments. GB is supported by the Helmholtz Association of National Research Centres.

[1] L. Bergström, Rep. Prog. Phys. **63**, 793 (2000).
[2] G. Bertone, D. Hooper, and J. Silk, Phys. Rep. **405**, 279 (2005).
[3] T. Appelquist, H.-C. Cheng, and B. A. Dobrescu, Phys. Rev. D **64**, 035002 (2001).
[4] G. Servant and T. M. P. Tait, Nucl. Phys. **B650**, 391 (2003).
[5] H.-C. Cheng, K. T. Matchev, and M. Schmaltz, Phys. Rev. D **66**, 056006 (2002).
[6] http://lhc.web.cern.ch/lhc/.
[7] E. A. Baltz, M. Battaglia, M. E. Peskin, and T. Wizansky, Phys. Rev. D **74**, 103521 (2006).
[8] A. K. Datta, K. Kong, and K. T. Matchev, Phys. Rev. D **72**, 096006 (2005).
[9] C. Munoz, Int. J. Mod. Phys. A **19**, 3093 (2004).
[10] F. Aharonian *et al.* (H.E.S.S. Collaboration), Phys. Rev. Lett. **97**, 221102 (2006); **97**, 249901(E) (2006).
[11] G. Zaharijas and D. Hooper, Phys. Rev. D **73**, 103501 (2006).
[12] S. Profumo, Phys. Rev. D **72**, 103521 (2005).
[13] Y. Mambrini, C. Munoz, E. Nezri, and F. Prada, J. Cosmol. Astropart. Phys. 01 (2006) 010.
[14] G. Bertone and D. Merritt, Phys. Rev. D **72**, 103502 (2005).
[15] A. Cesarini, F. Fucito, A. Lionetto, A. Morselli, and P. Ullio, Astropart. Phys. **21**, 267 (2004).
[16] A. Bouquet, P. Salati, and J. Silk, Phys. Rev. D **40**, 3168 (1989).
[17] J. Silk and A. Stebbins, Astrophys. J. **411**, 439 (1993).
[18] L. Bergstrom, J. Edsjo, and P. Ullio, Phys. Rev. D **58**, 083507 (1998).
[19] C. Calcaneo-Roldan and B. Moore, Phys. Rev. D **62**, 123005 (2000).
[20] R. Aloisio, P. Blasi, and A. V. Olinto, Astrophys. J. **601**, 47

(2004).
[21] S. M. Koushiappas, A. R. Zentner, and T. P. Walker, Phys. Rev. D **69**, 043501 (2004).
[22] J. Diemand, B. Moore, and J. Stadel, Nature (London) **433**, 389 (2005).
[23] L. Pieri, E. Branchini, and S. Hofmann, Phys. Rev. Lett. **95**, 211301 (2005).
[24] L. Pieri and E. Branchini, Phys. Rev. D **69**, 043512 (2004).
[25] E. A. Baltz, J. E. Taylor, and L. L. Wai, arXiv:astro-ph/0610731.
[26] P. Gondolo and J. Silk, Phys. Rev. Lett. **83**, 1719 (1999).
[27] G. Bertone, G. Sigl, and J. Silk, Mon. Not. R. Astron. Soc. **337**, 98 (2002).
[28] P. Gondolo, Phys. Lett. B **494**, 181 (2000).
[29] H. S. Zhao and J. Silk, Phys. Rev. Lett. **95**, 011301 (2005).
[30] G. Bertone, A. R. Zentner, and J. Silk, Phys. Rev. D **72**, 103517 (2005).
[31] D. Merritt, M. Milosavljevic, L. Verde, R. Jimenez, Phys. Rev. Lett. **88**, 191301 (2002).
[32] P. Ullio, H. S. Zhao, M. Kamionkowski, Phys. Rev. D **64**, 043504 (2001).
[33] D. Merritt, S. Harfst, and G. Bertone, Phys. Rev. D **75**, 043517 (2007).
[34] http://www-glast.stanford.edu.
[35] http://icrhp9.icrr.u-tokyo.ac.jp/.
[36] http://mpi-hd.mpg.de/hfm/HESS/HESS.html.
[37] http://hegra1.mppmu.mpg.de/MAGICweb/.
[38] http://veritas.sao.arizona.edu/index.html.
[39] http://www.mpi-hd.mpg.de/hfm/CTA/CTA_home.html.
[40] C. I. Fryer and V. Kalogera, Astrophys. J. **554**, 548 (2001).
[41] L. Ferrarese and H. Ford, Space Sci. Rev. **116**, 523 (2006).
[42] M. C. Miller and E. J. M. Colbert, Int. J. Mod. Phys. D **13**, 1 (2004).
[43] D. A. Swartz, K. K. Ghosh, A. F. Tennant, and K.-W. Wu, arXiv:astro-ph/0405498.
[44] X. Fan *et al.* (SDSS Collaboration), Astron. J. **122**, 2833 (2001).
[45] A. J. Barth, P. Martini, c. H. Nelson, and L. C. Ho, Astrophys. Lett. **594**, L95 (2003).
[46] C. J. Willott, R. J. McLure, and M. J. Jarvis, Astrophys. J. **587**, L15 (2003).
[47] Z. Haiman and A. Loeb, Astrophys. J. **552**, 459 (2001).
[48] R. Islam, J. Taylor, and J. Silk, Mon. Not. R. Astron. Soc. **340**, 647 (2003).
[49] S. M. Koushiappas, J. S. Bullock, and A. Dekel, Mon. Not. R. Astron. Soc. **354**, 292 (2004).
[50] M. Volonteri, F. Haardt, and P. Madau, Astrophys. J. **582**, 559 (2003).
[51] K. S. Thorne and V. B. Braginsky, Astrophys. J. Lett. **204**, L1 (1976).
[52] É. É. Flanagan and S. A. Hughes, Phys. Rev. D **57**, 4566 (1998).
[53] É. É. Flanagan and S. A. Hughes, Phys. Rev. D **57**, 4535 (1998).
[54] R. Islam, J. Taylor, and J. Silk, Mon. Not. R. Astron. Soc. **354**, 629 (2004).
[55] T. Matsubayashi, H. Shinkai, and T. Ebisuzaki, Astrophys. J. **614**, 864 (2004).
[56] S. M. Koushiappas and A. R. Zentner, arXiv:astro-ph/0503511.
[57] http://lisa.nasa.gov/.
[58] G. D. Quinlan, L. Hernquist, S. Sigurdsson, Astrophys. J. **440**, 554 (1995).
[59] J. F. Navarro, C. S. Frenk, S. D. M. White, Astrophys. J. **490**, 493 (1997).
[60] D. Merritt, arXiv:astro-ph/0301257.
[61] J. F. Navarro, E. Hayashi, C. Power, A. R. Jenkins, C. S. Frenk, S. D. M. White, V. Springel, J. Stadel, and T. R. Quinn, Mon. Not. R. Astron. Soc. **349**, 1039 (2004).
[62] N. Fornengo, L. Pieri, and S. Scopel, Phys. Rev. D **70**, 103529 (2004).
[63] J. J. Geehan, M. A. Fardal, A. Babul, and P. Guhathakurta, Mon. Not. R. Astron. Soc. **366**, 996 (2006).
[64] http://projects.hepforge.org/pythia6/.
[65] S. Kretzer, Phys. Rev. D **62**, 054001 (2000); www.pv.infn.it/%7Eradici/FFdatabase.
[66] L. Bergström, T. Bringmann, M. Eriksson, and M. Gustafsson, Phys. Rev. Lett. **94**, 131301 (2005).
[67] J. F. Beacom, N. F. Bell, and G. Bertone, Phys. Rev. Lett. **94**, 171301 (2005).
[68] T. Gaisser, M. Honda, P. Lipari, and T. Stanev, in Proc. of the 27th ICRC (2001).
[69] L. Bergström and D. Hooper, Phys. Rev. D **73**, 063510 (2006).
[70] http://wwwmagic.mppmu.mpg.de/physics/results/index.html.
[71] A. N. Cillis and R. C. Hartman, Astrophys. J. **621**, 291 (2005).
[72] http://heasarc.gsfc.nasa.gov/FTP/compton/data/egret/diffuse_maps.
[73] L. Bergstrom, J. Edsjo, and P. Ullio, Phys. Rev. Lett. **87**, 251301 (2001).
[74] J. E. Taylor and J. Silk, Mon. Not. R. Astron. Soc. **339**, 505 (2003).
[75] P. Ullio, L. Bergstrom, J. Edsjo, and C. Lacey, Phys. Rev. D **66**, 123502 (2002).
[76] S. Ando, Phys. Rev. Lett. **94**, 171303 (2005).
[77] S. Horiuchi and S. Ando, Phys. Rev. D **74**, 103504 (2006).
[78] E.-J. Ahn, G. Bertone, D. Merritt, and P. Zhang, Phys. Rev. D **76**, 023517 (2007).
[79] S. Ando, E. Komatsu, T. Narumoto, and T. Totani, Phys. Rev. D **75**, 063519 (2007).
[80] http://www-glast.slac.stanford.edu/software/IS/glast_lat_performance.htm
[81] G. Bertone, T. Bringmann, R. Rando, G. Busetto, and A. Morselli, arXiv:astro-ph/0612387.